Application of Gravity and Magnetic Techniques to Delineate the Subsurface Features in the Basement Complex in Imo Basin, Eastern Nigeria

Dagogo Franklin Ibim

Ignatius Ajuru University of Education, Rivers State, Nigeria

a b s t r a c t

The area of study is situated in the Nige r Delta . The current study is concerned with the analysis of magnetic and gravity data aiming to evaluate the subsurface structure of the basement rocks . The aeromagnetic and gravity methods of prospecting give an effective presentation of the subsurface structures . The aeromagnetic data was corrected and represented by total aeromagnetic intensity map then was reduced to the north magnetic pole . The corrected gravity data is represented by Bouguer anomaly map. The filtering techniques were applied to the corrected aeromagnetic and gravity maps to obtain the residual component caused by local structures and anomalies bodies . The integration of radially power spectrum was applied on both magnetic and gravity to estimate the depths of the shallow sources and the deep sources . The equivalent depths of the isolated short wavelength anomalies are 0.5 km and 0.4 km, and the depths of the long wavelength anomalies are 3.5 and 3 km for the magnetic and gravity data, respectively. The Euler deconvolution and 3-D modeling were applied to magnetic and grav- itydata . The 3-D Euler deconvolution is used not only to delineate major subsurface structures but also to determine the structural indices of them as well as the average depth of the magnetic and gravity sources . The calculated structural indices show that the area is mainly affected by contacts/thin sheet and the esti- mated depth of magnetic and gravity sources ranged between 500 m and 2000 m, also the 3-D Euler deconvolution showed that the area was affected by different fault trends such as NNE-SSW, NW-SE and E-W trends . The results of 3-D magnetic and gravity interpretation revealed that the depth of base- ment was ranging from 2500 m to 3000 m .The main tectonic deformations of the area of study have NNE-SSW, NW-SE and E-W trends .

1 . Introduction

The area of study of Magnetic data is situated in Central Sinai between two latitudes 2 9 ◦ 10 0 and 30 ◦ 40 0 N and two longitudes 33 ◦ 00 0 and 34 ◦ 30 0 E, covering an area 24, 163 km^2 . The Study area of gravity data is located also in Central Sinai between latitude 29 ◦ 45 0 N and 30 ◦ 15 0 N. and longitudes 33 ◦ 10 0 E and 34 ◦ 10 0 E, covering an area 5347 km^2 (Fig. 1). Integrated geophysical tools, aeromagnetic and gravity methods, are generally used in detecting the subsurface structures, the depth of the basement and, the sedimentary cover thickness . Several authors used integrated geophysical techniques at central Sinai area . Awad et al. (2001) utilized the gravity and deep seismic data to estimate the relation between the thickness of the crust and Bouguer anomalies ., Ghamry (2002) applied a geophysical study on El-Hasana area located in the northern part of central Sinai ., El-Bohoty et al. (2012) conducted comparative studies between the structural and tectonic situation interpreted from magnetic, gravity, and seismic data at the southern part of Sinai and red sea area, Egypt. Mekkawi et al. (2007) used magnetic

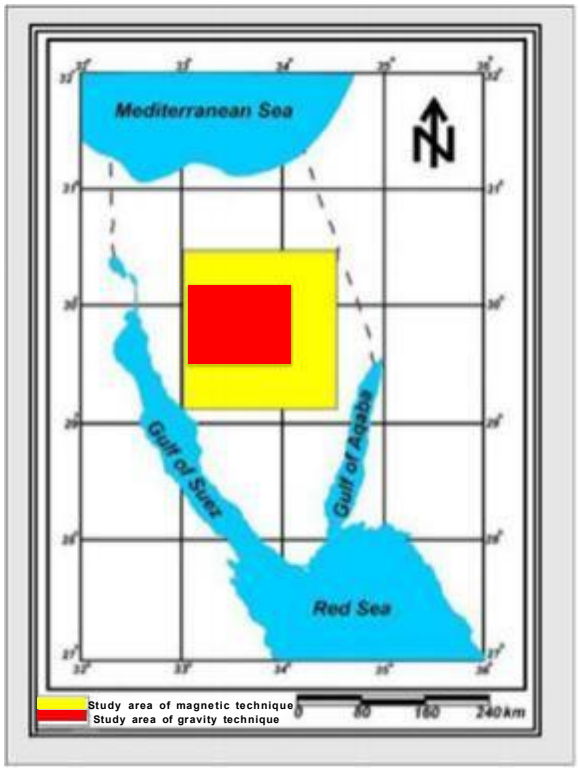

Fig. 1. Location map of the study area.

and magnetotulleric data to determine subsurface structure in the Hot Spring area, Central Sinai, Egypt. Sultan et al. (2009) applied geophysical techniques to image the subsurface and explore ground water at the central part of the Sinai Peninsula, Egypt. Rabeh (2011) designed a tectonic model of Sinai Peninsula depend- ing on the geophysical investigations. Se lim and Aboud (2012) in

their geophysical study on the center of Sinai Peninsula discussed the sedimentary cover overlaying the basement and the structural trends that crossing the area through using magnetic and gravity data analysis and Araffa et al. (2015) carried out a geophysical study on the central part of Sinai by using magnetic, gravity and geoelectric methods. This research illustrates an integrated geophysical study to estimate the geologic subsurface structures and the depth of the basement complex.

2. Geologic settings

The central part of Sinai Peninsula consists of two plateaus (El- Tih and El-Egma plateaus) which occupies 40 percent of Sinai and sloping northward toward Wadi El Arish. The maximum elevation of El-Tih Plateau is about 1600 m and decreases northward direction while El-Egma plateau lies to the north and has a maximum elevation of about 1650 m towards the south and decreases to 500 m northward. The study area is covered by sediments which were deposited on predominantly shallow platform and range from Cambrian to recent in age. In general, a thick sedimentary cover in Central Sinai that overlies the Precambrian basement rocks is morphologically forms the two outstanding El-Tih and El-Egma plateaus (Said, 1962). The geological map of the area of study (Fig. 2) shows several rock units of different ages and lithology (Modified after EGSMA, 1981). The succession of the stratigraphic strata in the area illustrated in (Fig. 3). Structurally, there are three main structural provinces distinguishing the Sinai Peninsula which are all involved in the central part of Sinai Peninsula.

From south to north these structural provinces are: stable shelf, transitional zone and unstable shelf, respectively. The first two provinces (stable shelf and transitional provinces) in which the study area is included occupy the plateaus of central Sinai, which are affected by NE- and NW trending faults. The last province (unstable shelf province) is affected by fold-belt of the Syrian Arc System which northly ended by the E–W trending Nile Delta Hinge zone.

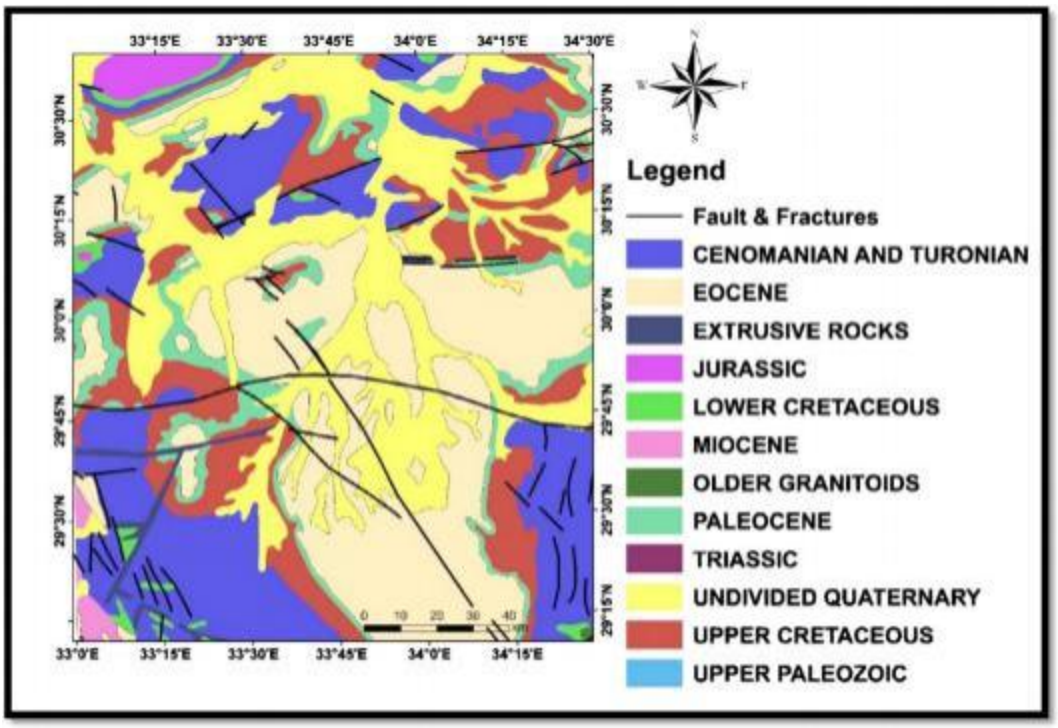

Fig. 2. Geologic map of the study area shows the main geological formations of the surface (Modified after EGSMA, 1981).

3. Methodology

In the present study, two geophysical techniques were conducted in the study area including aero magnetic data which was prepared and compiled by (Folkman and Assael, 1980) and gravity data that was used after (Ismail et al., 2001). For the purposes of evaluating the subsurface structures in the studied area.

3.1. Magnetic Method

The magnetic method is one of the most widely used geophysical techniques for investigating the subsurface of the Earth. It can be applied to a wide variety of subsurface exploration problems including horizontal magnetic variations from Earth's crust base to within the uppermost meter of soil. These variations cause anomalies in the Earth's normal magnetic field that are mapped by the magnetic method (Hinze et al., 2013). The magnetic method depend on variations in the earth magnetic fieldderived from lateral differences in the magnetization of the subsurface (Hinze et al., 2013).

3.2. Gravity method

The gravity method depend on the measurement of variations in the gravity field caused by horizontal variations of density in the subsurface. It is the essential method in number of specific geological studies, as in mapping near surface voids, quantitative studies of metallic ore bodies, characterizing salt structures, and

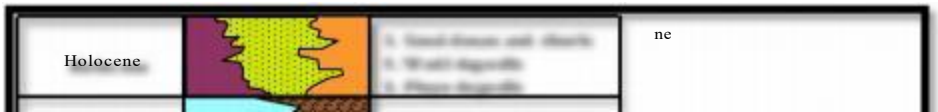

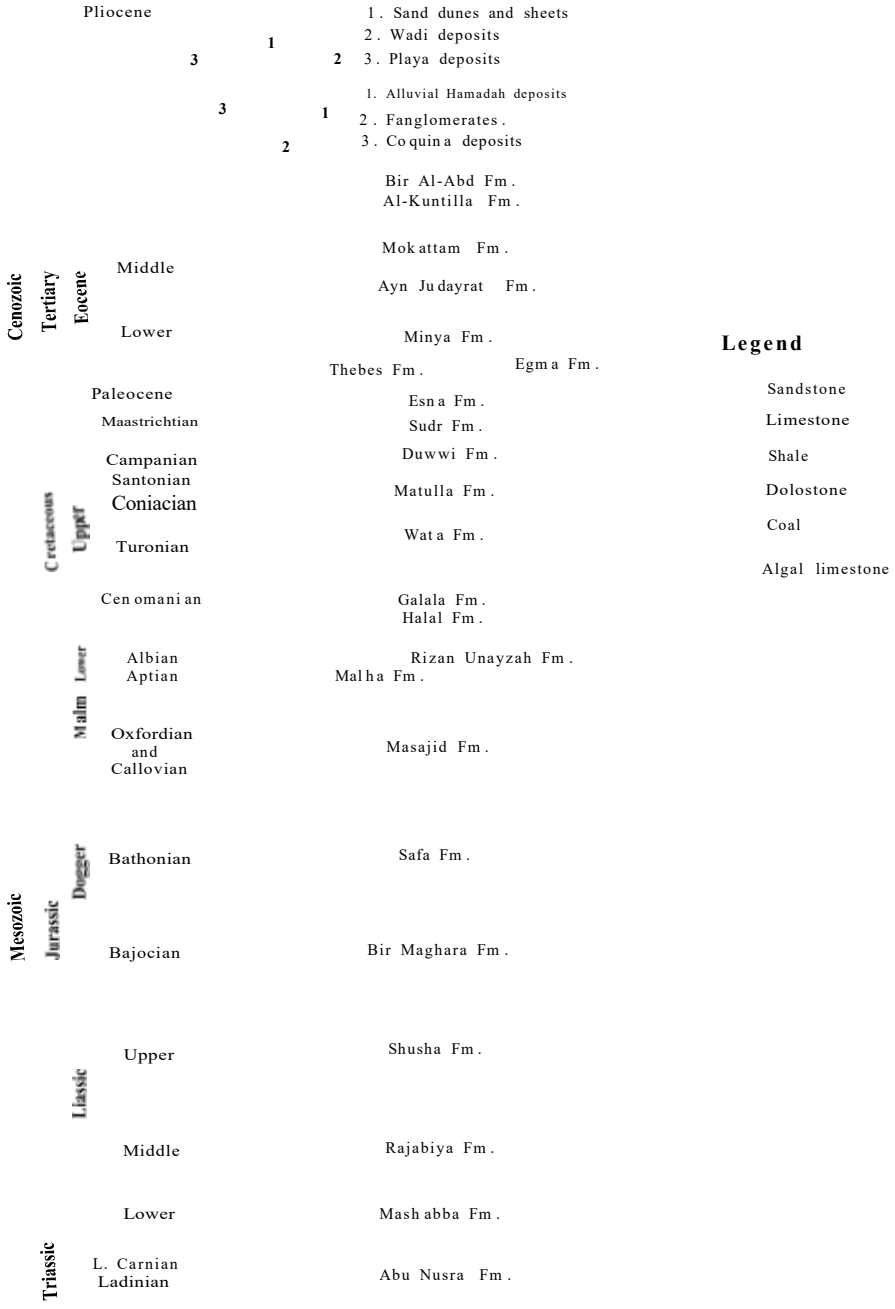

Fig. 3. Generalized stratigraphic column of north and central Sinai (compiled after EGSMA, 1992, 1993 and 1994).

monitoring changes of fluid/gas content in volcanoes. The gravity method has also been used in regional characterization of the earth to determine the structures of the crust, identifying potentially favorable regions for resource exploration, and developing conceptual exploration models (Hinze et al., 2013).

4. Potential field data interpretation

4.1. The reduced to the north magnetic pole (RTP) map

From outlook of the total intensity aeromagnetic map (Fig. 4a) and the RTP aeromagnetic map (Fig. 4b) we note that the northward shift of the implied anomalies of the effect of the inclination of the magnetic fieldat the study area. Also the number of anomalies becomes larger with comparable decrease of their ariel extension and the increase of their vertical relief.

From the analysis of the RTP aeromagnetic anomaly of the investigated area as shown in (Fig. 4b), indicates that the magnetic fieldin the area has a maximum relief of about 600 nT nearly in the northern part and minimum relief of about 300 nT in the central part of the map. These anomalies have different shapes, polarities and reliefs. The general magnetic trends pattern of this field are NNW-SSE, NE-SW, and E-W. In the northern part of the map, the anomalies consists of three closures, two of them having polarities are characterized by its positive polarities, irregular shape, moderate gradient and trending NW-SE, between these closures the area of low anomalies (negative polarity) are located and consists of one closures of irregular shape, moderate gradient that is trending in NW-SE direction. The southern flank of these anomalies, however are superimposed by another magnetic anomalies features of negative polarity and high gradient. The elongated anomaly zones with high gradient indicate considerable subsurface faulting trend-

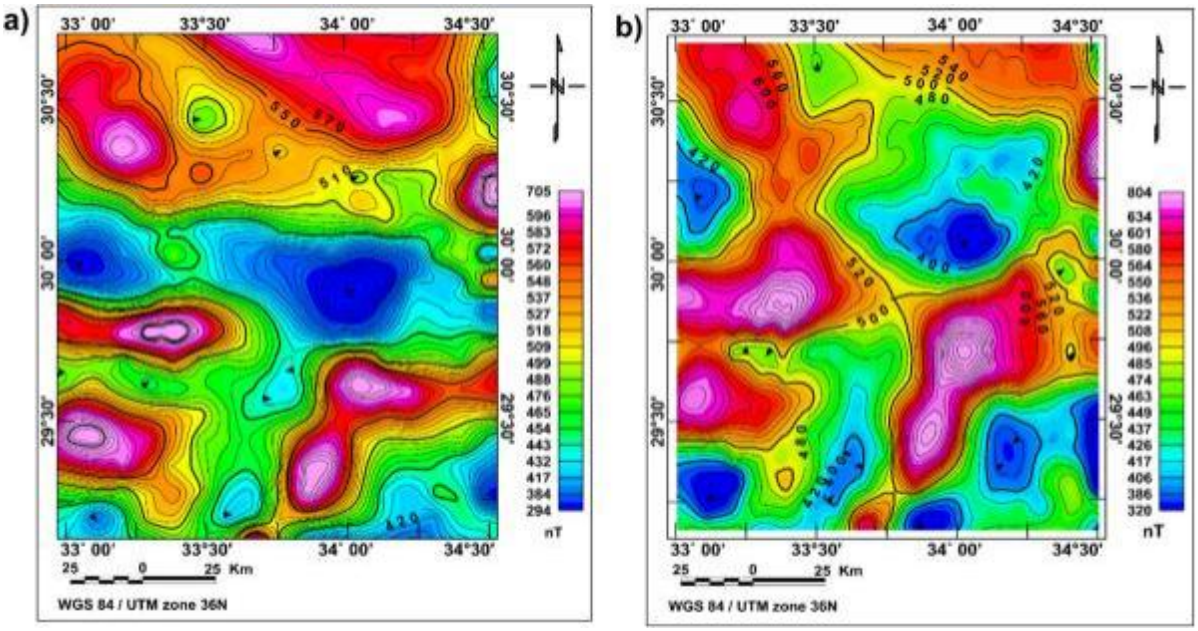

Fig. 4. (a) Total aeromagnetic anomaly map of the study area (Modified after Folkman and Assael, 1980). (b) RTP aeromagnetic anomaly map of the study area.

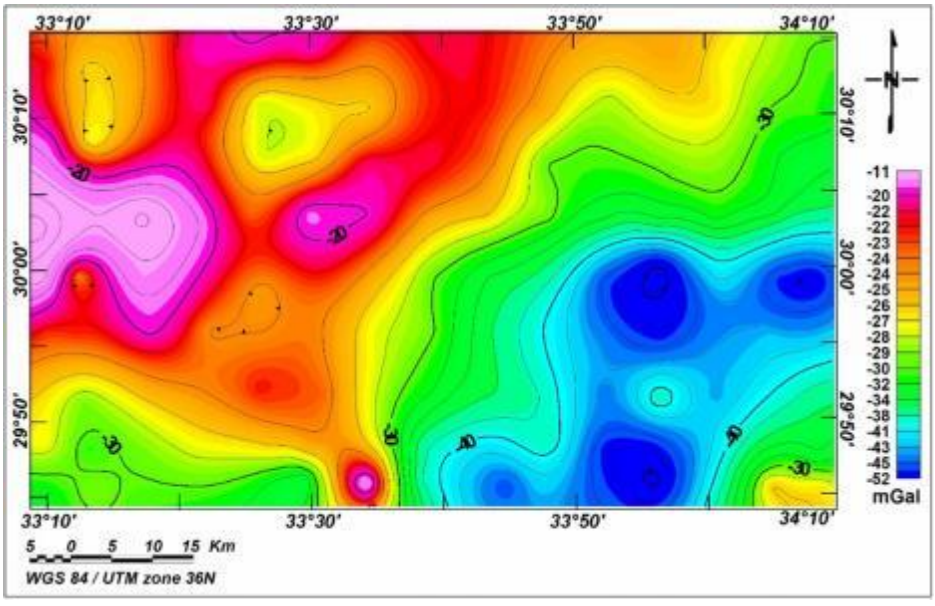

Fig. 5. Bouguer anomaly Map of the Study Area.

ing NW-SE. These anomalies can be explained as the result of magnetic basaltic extrusions associated with the NW-SE faulting trend. Further south, the anomalies are ellipsoidal of low anomalies (negative polarity). They are characterized by moderate sharpness and moderate gradient, the general magnetic trends pattern along this part are NE-SW, and NW-SE. This anomaly represents a shallow sedimentary basin.

4.2. Bouguer gravity anomaly map

The Bouguer anomaly map (Fig. 5) indicates lateral changes in the earth gravity field which has a maximum anomaly value of about -11 mGal at the northern and northwestern parts but minimum anomaly value of about -52 mGal at the southern, southeastern and at the southwestern parts of the study area. High gravity anomalies are concentrated in the northern, northwestern and nearly in the southwestern parts of the area of study. In general these high gravity anomaly zones may be due to the presence of subsurface denser rocks or due to shallower or near surface uplifted blocks of basement rocks. Low gravity anomalies are concentrated in the eastern, and in the southeastern parts. Generally the negative gravity anomalies are probably due to presence of thick sedimentary sections in these parts of the study area.

4.3. Radially averaged power spectrum technique

This technique is used to detect the depths of the shallow depths, basement complex, and the subsurface geological structures. Several authors, such as Bhattacharya (1994), Spector and Grant (1970). Garcia and Ness (1994), Muririzio, Tatiana and

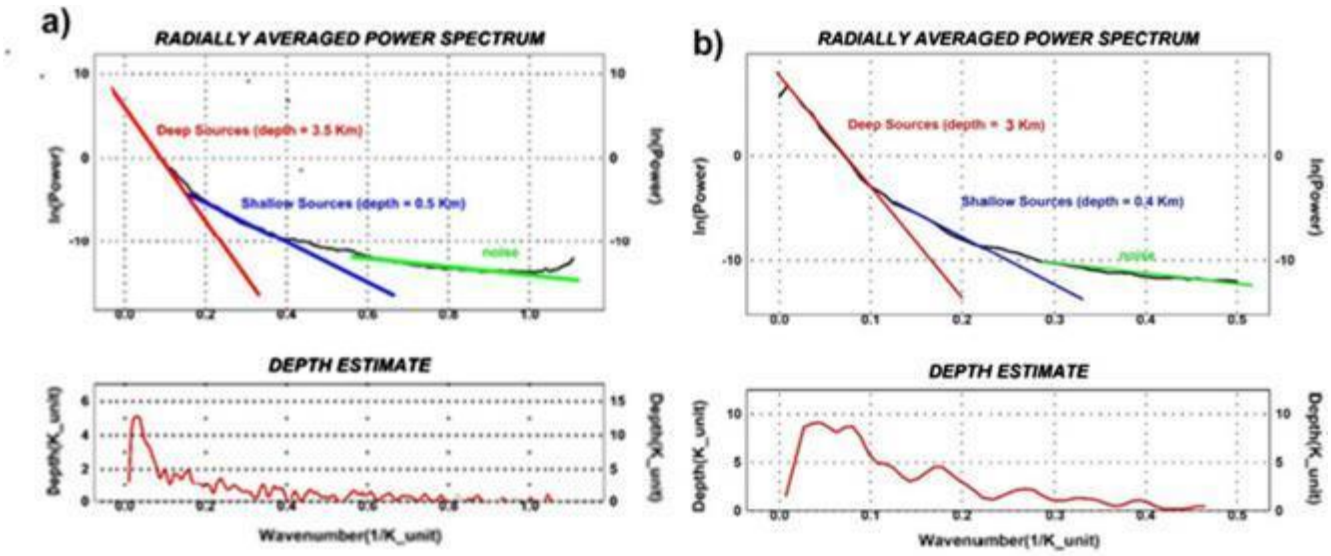

Fig. 6. (a) 2-D radially averaged power spectrum for the magnetic data. (b): 2-D radially averaged power spectrum for the gravity data.

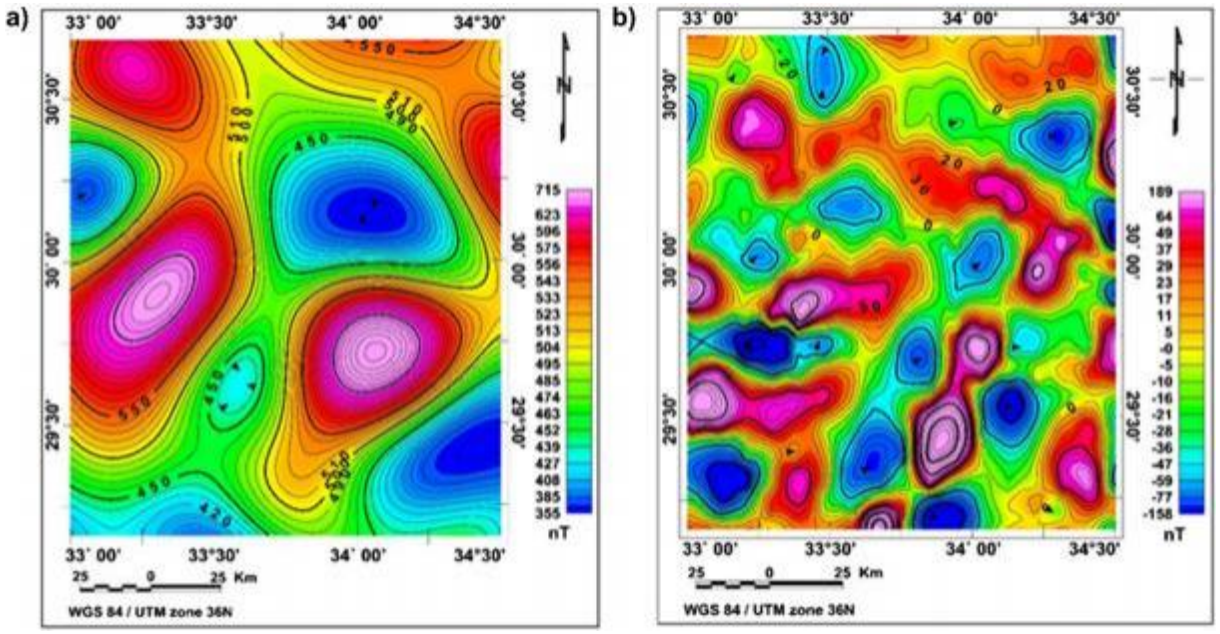

Fig. 7. (a) Low pass magnetic filter map with effective cutoff wave length of 0.0169 cycle/unit. (b) High pass magnetic filter map with effective cutoff wave length of 0.0169 cycle/unit.

Angelo (1998), explained the spectral analysis technique. It relies on the analysis of the magnetic data using the Fourier Transform on the spectral analysis map and its computer conjugate. It is a function of wavelengths in both the X and the Y directions. In the present work, we applied the Fast Fourier transform (FFT) on both RTP aeromagnetic data and gravity data, to calculate the energy spectrum. 2-D radially averaged power spectrum technique has been applied to determine the average depth level to the mag-

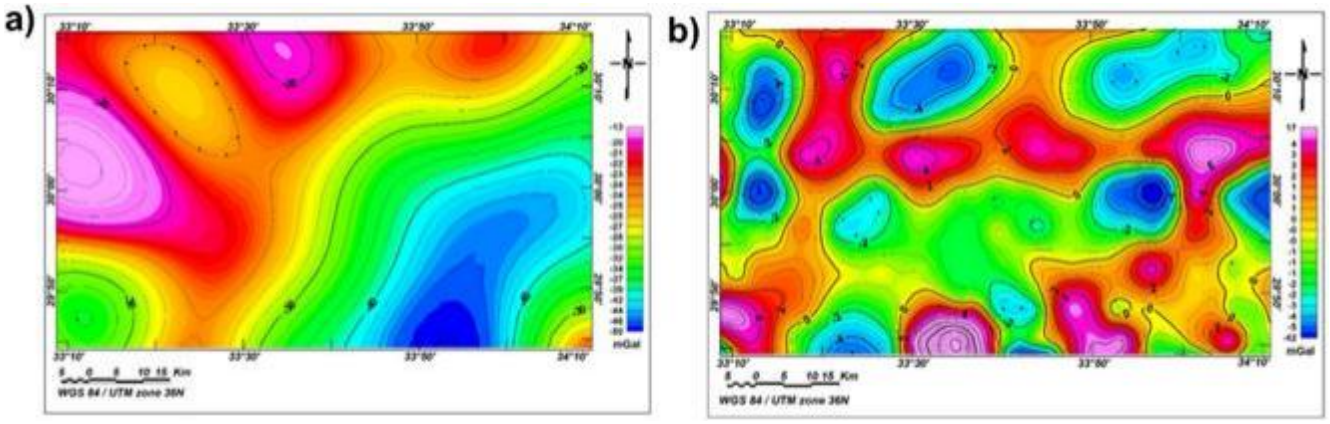

Fig. 8. (a) Low pass gravity filter map with effective cutoff wave length of 0.0285 cycle/unit. (b) High pass gravity filter map with effective cutoff wave length of 0.0285 cycle/unit.

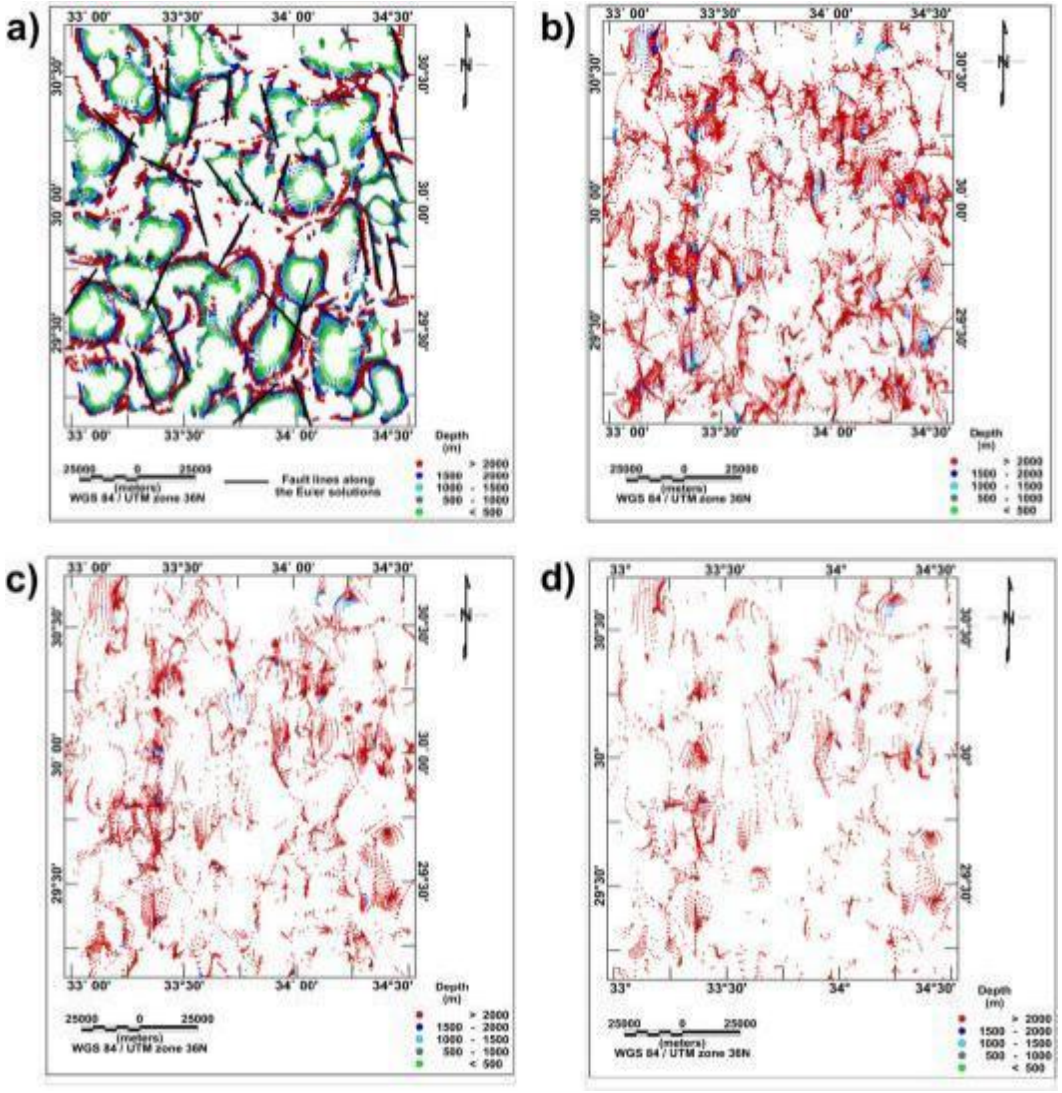

Fig. 9. (a) Euler Solutions of the RTP magnetic map of Structural Index = 0. (b) Euler Solutions of Structural Index = 1. (c) Euler Solutions of Structural Index = 2. (d) Euler Solutions of Structural Index = 3 for magnetic data.

netic and gravity source in the studied area. In this work such technique was applied for both of magnetic and gravity data, using (Oasis Montaj Program v.8.4, 2015). The obtained diagrams of the radially power spectrum Fig. 6a and Fig. 6b illustrate the estimated average depth levels to the deep and shallow depth segments prevailing the study area. The 2-D power spectrum diagram of the magnetic data. (Fig. 6a) indicates, that the deeper source has an average depth of about 3500 m and the shallow is of about 500 m. However, the estimate the average depth of the gravity source bodies (Fig. 6b) is 3000 m for the deep and 400 m for the shallow source. It is noted that the average depth of the deeper magnetic data is more than gravity, as it somewhat directed to the basement surface as well as intra basement source. Also the application of this method gives an accurate picture of the depth in the two-dimensions of the digitized magnetic and gravity data.

4.4. Filtering techniques

The main aim of the filtering techniques is to separate the anomalies of different wavelengths from each other. The local anomalies of shallow sources are corresponding to the anomalies of short wavelengths or high frequencies while the regional anomalies of deep sources are corresponding to long wavelengths or low frequencies.

In this work, the 2-D filtering was carried out on the RTP aeromagnetic maps, and Bouguer map to the lineation caused by structural faulting or dislocations in the basement rocks at different depths. In the present study, the filtering technique is performed using the frequency ranging between 0.0169 cycle/ unit and 0.0285 cycle/ unit data.

Through low pass magnetic filtered map of the study area shown in (Fig. 7a) with an effective cutoff wavelength of 0.0169 cycle/ unit, we find that the magnetic field increases in the northeastern and southwestern with the prominent trends is NE-SW. and NW-SE The prominent Structure trends in the RTP magnetic map (Fig. 4b), is still found in the low pass filtered map and, this reflects the tectonic nature of these faults and subsurface structures which extend from shallow depths and even great depths. We note also that the local structures in the Northwestern and Southwestern parts.

The high pass filter applied on the magnetic map of studied area with effective cutoff wavelength of 0.0169 cycle/ unit (Fig. 7b) indicates short wavelength spot and high frequency like magnetic anomalies which map are inferred as residual component located in the southeastern and southwestern parts of the studied area. Also the map contain a large numbers of smaller anomalies resulted from the filtering process. However, the prominent trends in the magnetic map is NE-SW and NW-SE is still found in the high filtered map and this indicates that the prevailing faults trends (RTP map, Fig. 4b) expanded in the subsurface of the study area up to shallow depths. Furthermore, the random trends of small scale anomalies illustrating that the shallow subsurface section has been dissected by different stresses of the new tectonics that may have not affected.

Through careful analysis of low pass gravity filtered map (Fig. 8a) with cutoff at 0.0285 cycle/ unit .Clear that, the prominent NE-SW, and NW-SE, anomalies trends still persist, which reflects the deep extent of the subsurface structures causing these faults anomalies. This demonstrates the depth of textures responsible for the presence of these faults, which interpreted the extended of these faults to great depths. However, some smooth regional anomalies that appear not to be related to a subsurface structure arc most probably a result of regional variation in the density of the rocks at high depth.

The high pass gravity filtered map of the study area is shown in (Fig. 8b) with an effective cut-off wavelength of 0.0285 cycle/ unit, reveals three structural features indicated by linear anomalies having their extension in an NE-SW, E-W, and N-S direction. These Linear anomalies border several local anomalies of different shapes and polarities (positive and negative). The most significant features are the major anomalies of different shape, and polarities which extend downward s of the basement itself in E-W direction at central, eastern, north-western parts. The negative polarities control a zone of uplifting striking faults in north, south and western blocks having extension E-W and N-S direction. These faults have the main trends E-W, NW-SE and N-direction and affected also on the overlain sedimentary section.

4.5. Depth estimation

4.5.1. Euler deconvolution

The Euler deconvolution technique was first applied on the profile data by (Thompson, 1982) which later advanced by

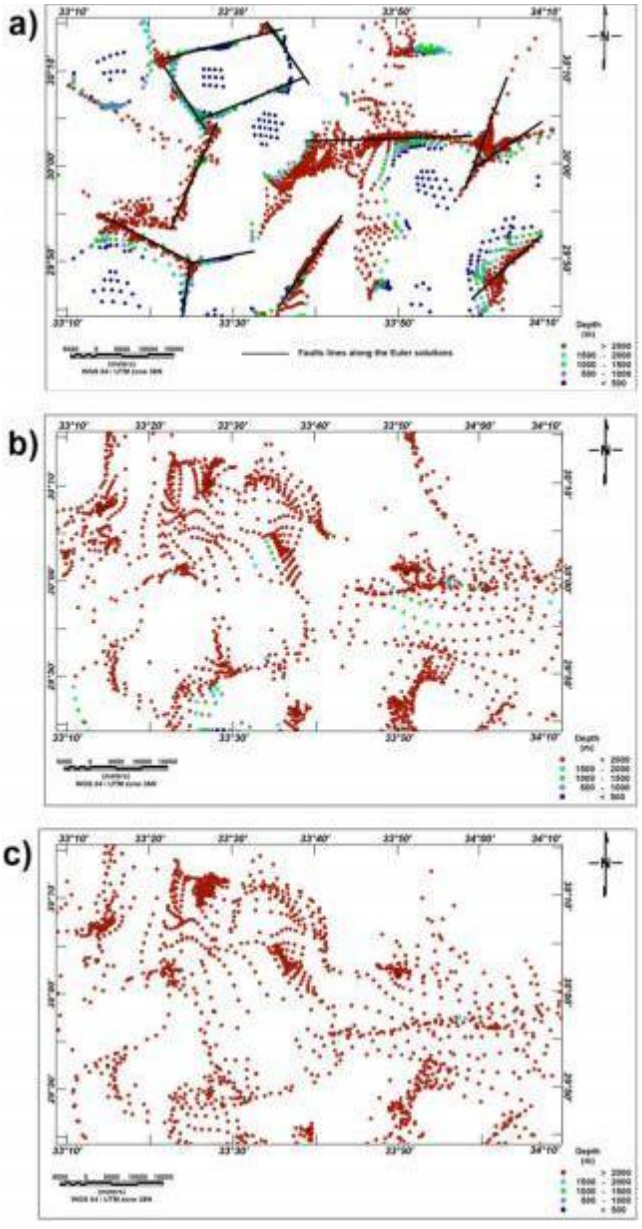

Fig. 10. (a) Euler Solutions of the Bouguer anomaly map of Structural Index = 0. (b) Euler Solutions of Structural Index = 1. (c) Euler Solutions of Structural Index = 2 for gravity data.

(Reid et al., 1990) for the gridded data. Euler deconvolution method is used to estimate the locations and depths for several linear subsurface features such as (lineaments, geological contacts, faults, dikes, sills). So that, it requires knowledge about the type and nature of the causative body which can be achieved by defining the structural index (Salem et al., 2008). Moreover, the structural index can be defined as the rate of change of the field depending on the source geometry. In the present study, the 3-D Euler deconvolution technique was applied on both magnetic and gravity field data in order to detect the locations and depth values of the different lineaments and faults in the study area.

The obtained Euler deconvolution solution of the magnetic map Fig. 9. The Euler solutions are applied to the RTP magnetic map of the studied area using the (Oasis Montaj Program v.8.4, 2015). In the present study the structural index that applied to RTP map are 0, 1, 2, and 3 to select the best solution. RTP magnetic map at SI = 0 as in (Fig. 9a), SI = 1 as in (Fig. 9b), SI = 2 as in (Fig. 9c) and SI = 3 as in (Fig. 9d). The structural index SI = 0 gives better solutions than structural index 1, 2, and 3 because the data are concentrated at some places in the study area not distributed all over the area as SI = 1, SI = 2 and SI = 3.

In gravity data Euler deconvolution solution was applied to Bouguer anomaly map for various structure indexes (SI). If the structural index = 0 (Fig. 10a), it indicates to dyke, sill, step, and ribbon. If the structural index = 1 (Fig. 10b), it indicates to pipe and cylinder. If the structural index = 2 (Fig. 10c), it indicates to sphere (Oasis Montaj Program v.8.4, 2015). Euler deconvolution method was applied on the study area by using Structural index (SI) = 0, 1, and 2 to achieve different solutions (Fig. 10). Fig. 10a (SI = 0) indicates the best comparable fault system.

It is obvious that, the depth values of the fault structures or contacts structures obtained from both Euler deconvolution of magnetic and gravity data in the study area ranging from minimum depth value of less than 500 m to maximum depth value of more than 2000 m, and the subsurface lineaments and fault structures are oriented in different directions such as NNW-SSE, NE-SW and E-W taking the trends of the Gulf of Suez, Gulf of Aqaba and Syrian arc folding system and offshore Mediterranean coastal zone respectively.

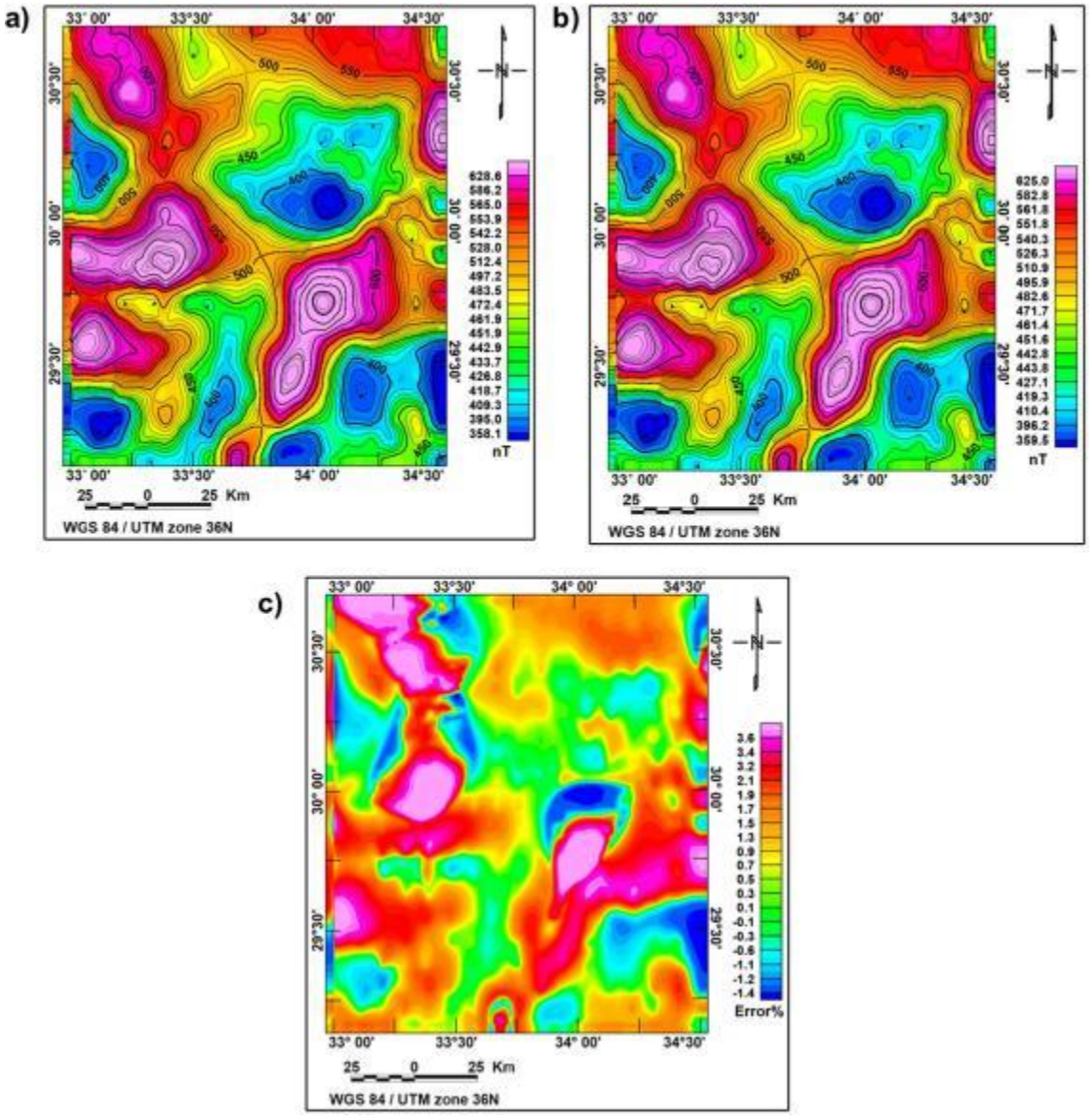

Fig. 11. (a) Observed magnetic anomaly. (b) Calculated magnetic anomaly. (c) Error percentage.

4.5.2. 3- D magnetic modeling

The interactive 3-D magnetic and gravity modeling software program is designed for performing layer-earth models. Hence, the GM-SYS 3D is an extension for Oasis Montaj Program v.8.4, 2015 which is used for the purpose of 3-D modeling of subsurface structures and detecting the depth to the top of the basement surface, prevailing the studied area.

In the present work, for the magnetic data, the 3-D magnetic modeling was carried out by applying ten iterations until the fitting between the observed and calculated magnetic data occurred with error percentage lower than 5 percent (Fig. 11a–c). The obtained results show that the two main parts of the Final 3-D magnetic modelling (Fig. 14) are topographic surface as shown in Fig. 12a and the upper crust (the depth to the basement rocks) as shown in Fig. 12b. 1 – The topographic surface (Fig. 12a) ranges between 140 m in the northern and northeastern parts and 990 m in the central, southwestern parts of the study area, forming high topographic features. 2 - The upper crust (the depth to the basement rocks), from the analysis of the depth to the basement surface map in the studied area (Fig. 12b) we can note that the depth of the shallow basement surface located in the northwestern and central parts of the study area approximately equals to 2.5 km, below the sea level. While the deep basement surface is concentrated in the eastern, southwestern and northeastern parts of the study area relatively equals to 3 km. From the results of the depth to the basement we can deduce that the thickness of thesedimentary cover ranges from 2.5 km in northwestern and central parts and 3 km in southeastern and southwestern parts. Fig. 13 shows the 3-D magnetic modeling of the basement surface of the study area Fig. 16 shows the final 3-D magnetic modeling of the study area.

For gravity data, the 3-D gravity modeling was carried out by applying ten iterations until the fitting between the observed and calculated gravity data occurred with error percentage lower than 0.5 percent (Fig. 15a–c). The most important results of the final 3-D gravity model are discussed here unit-wise in connection with the existing geophysical results of the study area and the adjoining regions. 1 – The topographic surface, this surface is ranging from minimum value of about 313 m in the northeastern parts of the studied area to maximum value of about 631 m in the southern and eastern parts (Fig. 16a). 2 – The upper crust (The depth to the basement surface), this surface which is considered here at the bottom of the sedimentary layer. The basement relief of gravity map (Fig. 16b) clears that the depth of the basement surface equals to 2500 m which represents the shallow depth and is located in the northeastern part of the studied area and the deeper basement surface with depth values about 3000 m below the sea level toward the southeastern and southwestern parts of the study area. In general, the thickness of the basement layers increases towards the

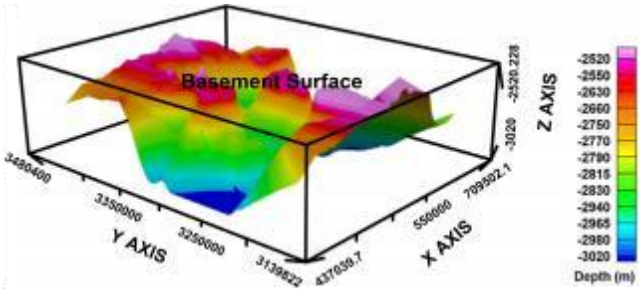

Fig. 13. 3-D magnetic modeling of the basement surface of the study area.

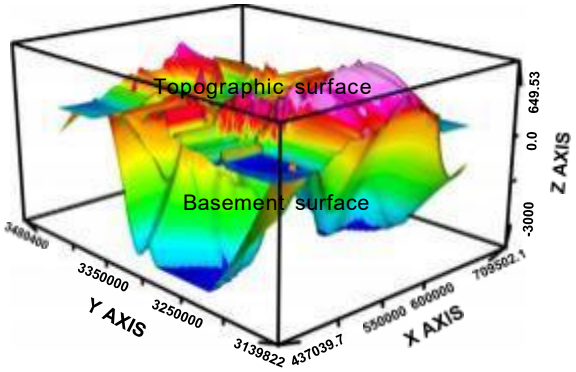

Fig. 14. Final three-dimensional (3-D) Magnetic modeling of the study area.

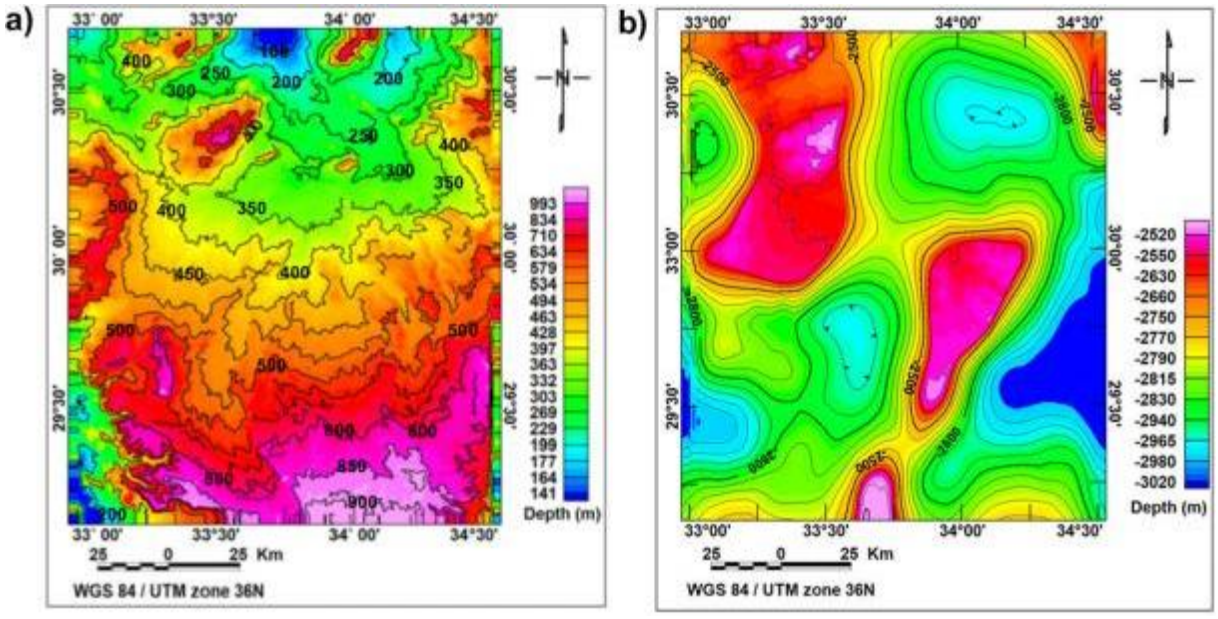

Fig. 12. (a) Surface topographic map of the study area. (b) Basement relief magnetic map, below the sea level of the study area.

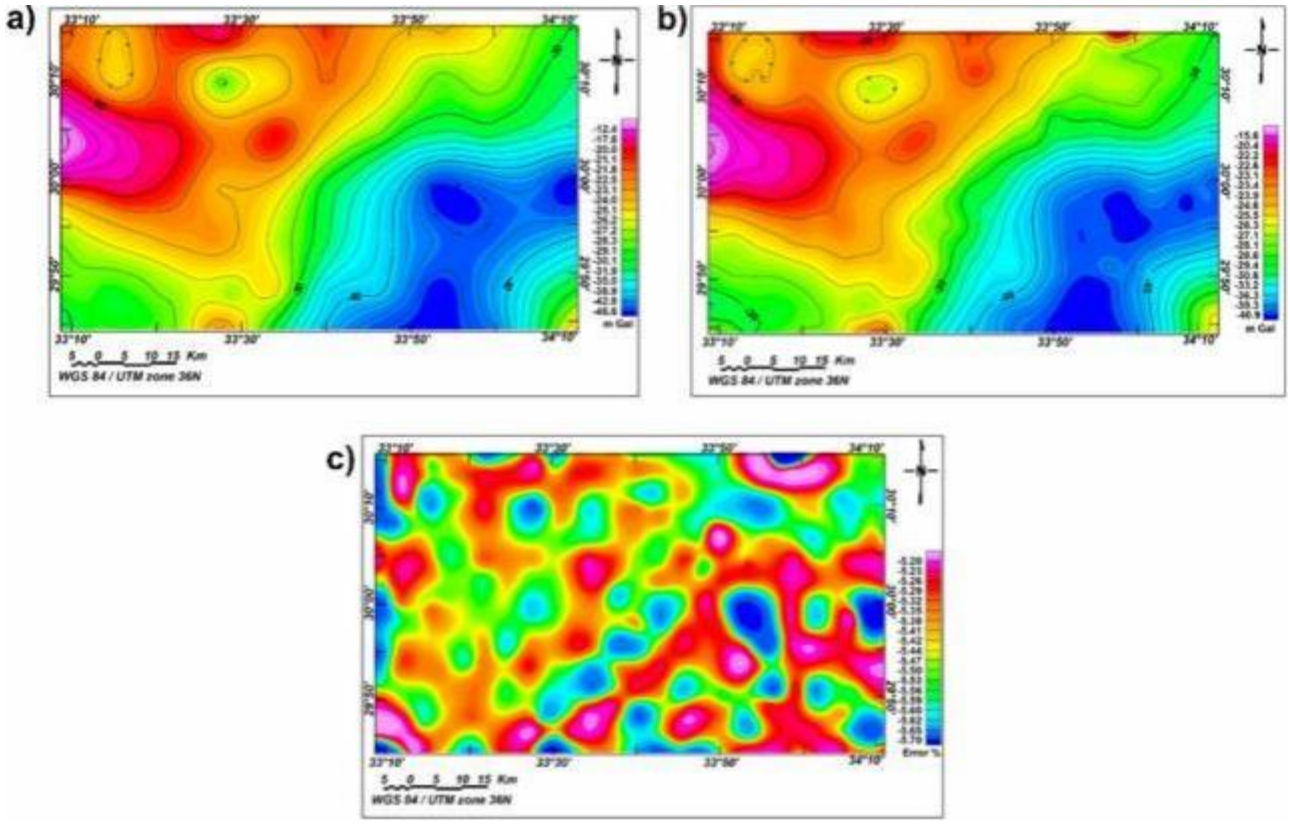

Fig. 15. (a) Observed gravity anomaly. (b) Calculated gravity anomaly. (c) Error percentage.

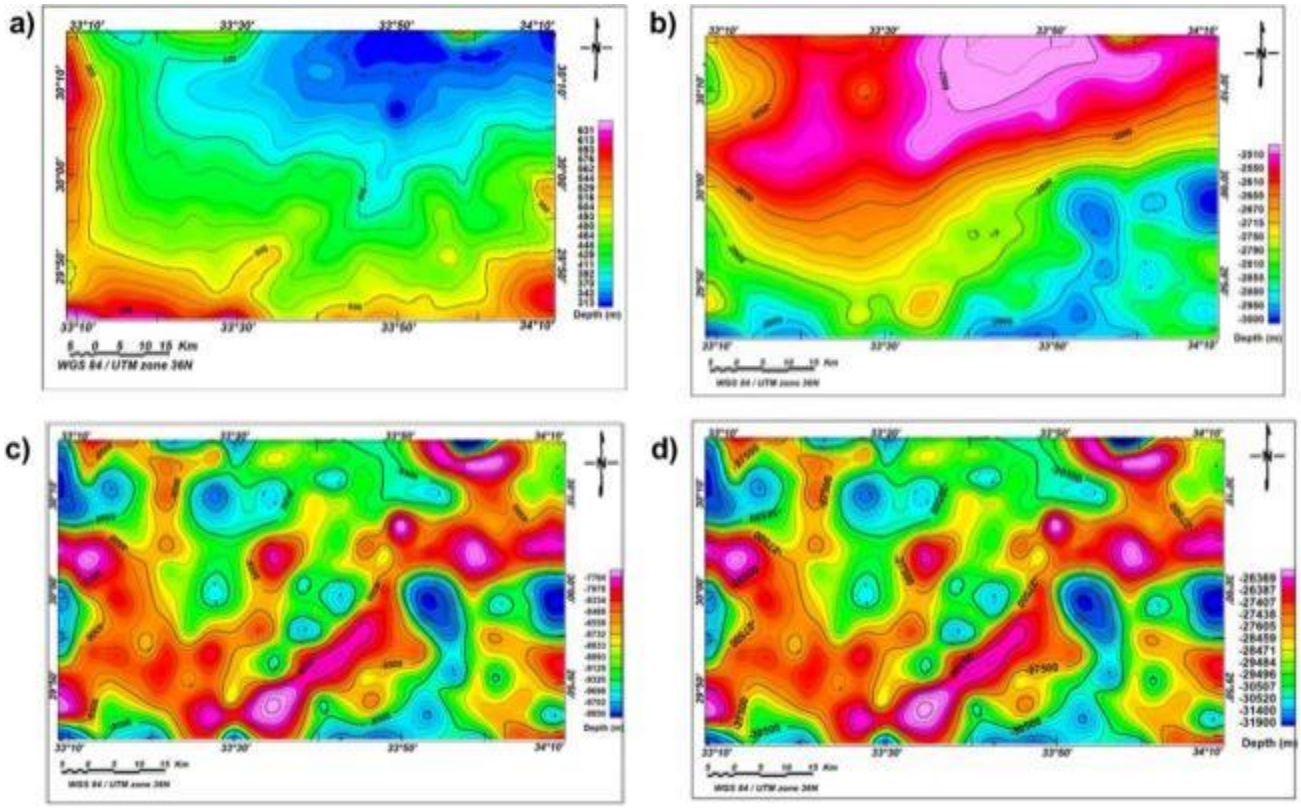

Fig. 16. (a) Surface topographic map of the study area. (b) Basement relief gravity map, below the sea level. (c) Conorad map, below the sea level. (d) Moho map, below the sea level of the study.

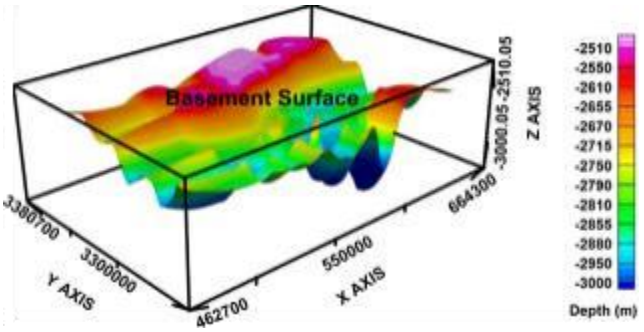

Fig. 17. 3-D gravity modeling of the basement surface of the study area.

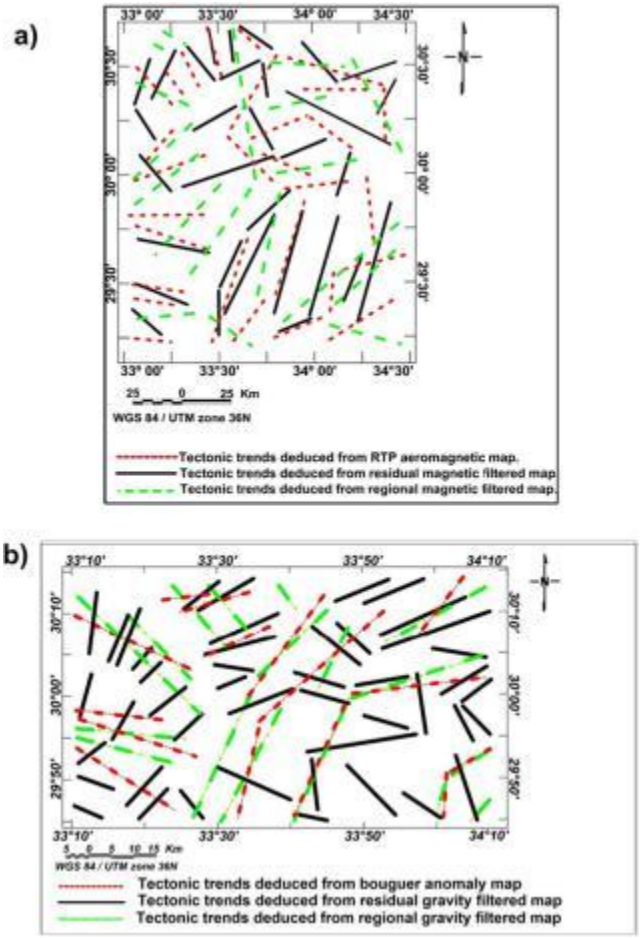

Fig. 18. (a) A map showing tectonic trends deduced RTP aeromagnetic map, residual magnetic filtered map and regional magnetic filtered map. (b) A map showing tectonic trends deduced Bouguer anomaly map, residual gravity filtered map and regional gravity filtered map.

southern part of the study area. Fig. 17 shows the 3-D gravity modeling of the basement surface of the study area. 3 – The middle crust (Conrad surface), this surface shows the top of the oceanic crust with relatively depths ranging from 7764 and 9850 km (Fig. 16c). 4 – The lower crust (Moho surface), this surface (Fig. 16d) is a relatively ranging from 26.4 to 31.9 km in the study area.

4.6. Structural analysis

The RTP aeromagnetic, Bouguer gravity maps and filtered magnetic and gravity anomaly maps, (Figs. 4b, 5, 7 and 8) were used to

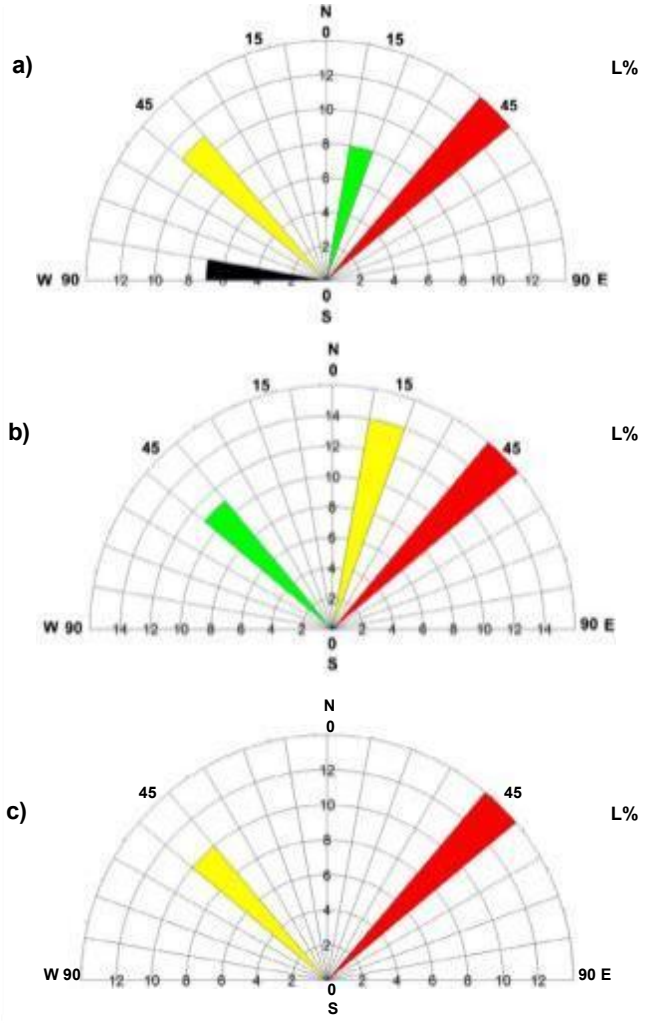

Fig. 19. Rose diagrams deduced from: (a) RTP aeromagnetic map. (b) High pass magnetic filtered map. (c) Low pass magnetic filtered map.

determine the general structural trends in the studied area, by applying Linsser (1967) technique. Linsser (1967) stated that mapping the structural trends by following lineation in magnetic contour represent the most useful geological applications of magnetic surveys. In some situations the lineations reflect the strike lines of elongated intrusive features or the surfaces of large faults reflected in the basement topography. Such features are concealed under sedimentary layers and show up only on the magnetic maps.

The deduced structural maps (Fig. 18a and b) represent the fault system dissecting the area. The deduced fault planes of the different directions are grouped every 10 ◦ around the north for their length percentage L% and represented by Rose diagrams. The results of fault system deduced from both magnetic map, gravity and filtered magnetic and gravity anomaly maps, were represented in the form of rose diagram as shown in (Figs. 19 and 20).

The results indicate that, most of the predominant directions are N 45 ◦ E this trend is the most predominant direction in the investigated area according to its characteristics making a mean strike of N 45 ◦ E. This trend has a strong relation to trends deduced from RTP magnetic maps and Bouguer anomaly maps. The second predominant trend is N 45 ◦ W which is related to Gulf of Suez trend. The third predominant trend is N 15 ◦ E trend that is related to River- Nile system. The least predominant is the E-W trend that related to the Mediterranean tectonics. It can be stated that the area has been affected mainly by Gulf of Aqaba as well as Gulf of Suez and Syrian Arc tectonics.

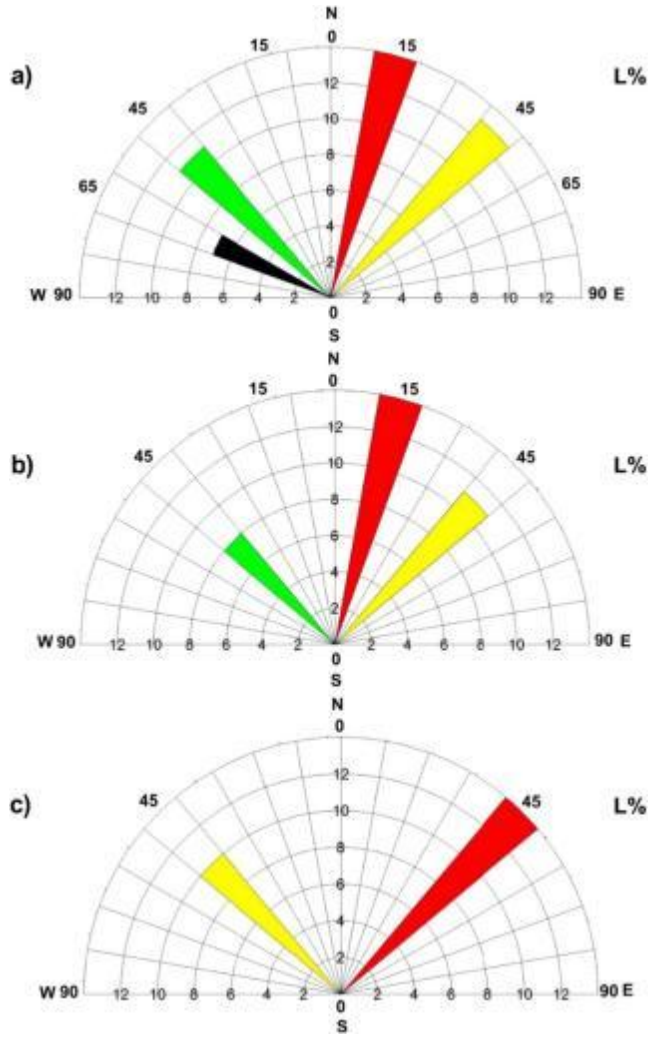

Fig. 20. Rose diagrams deduced from: (a) Bouguer anomaly map. (b) High pass gravity filtered map. (c) Low pass gravity filtered map.

5. Discussion

This study aims to determine the structural element which affected the study area. Magnetic and gravity data interpretation are used to determine subsurface structures and define the depth of the basement complex. The trends of fault elements which were deduced from RTP, Bouguer anomaly map and the filtered magnetic and gravity maps are integrated with the results of Euler deconvolution as shown in (Figs. 4b, 5, 7, 8, 9 and 10). The magnetic and gravity data interpretations indicate that the Euler solutions for depth increase towards the middle and northeast parts of the study area. The central and northeastern parts reveal high depths, the results of magnetic and gravity interpretation using Euler solutions indicate that the depth of basement ranges between 500 m and 2000 m (Figs. 9 and 10). There is a good agreement between the results of the 3-D magnetic and gravity modeling. The results of 3-D magnetic and gravity modeling show good fitting between observed and calculated data (Figs. 13 and 17). Also, the results of the 3-D magnetic and gravity modeling reveal the position of the different layers (Figs. 11 and 15). The topographic surface of magnetic data which ranges from 141 m to 993 m above sea level is shown in (Fig. 12a) while the topographic surface of gravity data (Fig. 16a) ranges from 313 m to 631 m above sea level. The depth of the of basement complex based on magnetic and gravity interpretation ranges between 2500 m to 3000 m, as shown in (Figs. 12b and 16b).

6. Conclusions

The objectives of this study are to evaluate the subsurface tectonic pattern, and to study the basement relief and its tectonics in the studied area. The most important conclusions reached in this study are:

- From the RTP aeromagnetic map of the studied area, the southern, northwestern and northeast parts have thick sedimentary cover and huge depth of basement rocks.
- From the Bouguer anomaly map of the studied area, the eastern, and the southeastern parts have huge depth of basement rocks which indicate on thick sedimentary cover.
- The depth of basement rocks in the studied area ranging from 1000 m to 2000 m.
- The Euler deconvolution technique has been also applied for the grided magnetic and gravity data to estimate basement depth as well as its structural deformations. The obtained Euler anomalies depths range from <500 m to >2000 m.
- The interpreted subsurface structural elements dissected the study area were oriented into three different major directions such as NE-SW, NW-SE and E-W trends. It can be stated that the area has been affected mainly by the Gulf of Aqaba as well as Gulf of Suez, and Syrian arc tectonics. Finally, the obtained result from this geophysical study could contribute for the understanding of the subsurface structural settings and the basement relief and tectonics of the Central Sinai area.

References

Araffa, S.A.S., Sabet, H.S., Gaweish, W.R., 2015. Integrated geophysical interpretation for delineating the structural elements and groundwater aquifers at central part of Sinai Peninsula Egypt. J. Afr. Earth Sc. 105 (2015), 93–106.

Awad, M.B., El-Gendy, A., El-Ghamri,M.A., Hussein, S.A., Hamouda, A.Z., 2001. Neotectonics of the Gulf of Aqaba, Red sea, interpreted from gravity and deep seismic data. In: Proc. 2nd International Symposium on Geophysics, Tanta, pp. 13–26.

Bhattacharya, J., 1994. Cretaceous Dunvegan formation of the Western Canada Sedimentary Basin. In: Mossop, G.D., Shetsen, I. (comp.), Geological Atlas of the Western Canada Sedimentary Basin, Canadian Society of Petroleum Geologists and Alberta Research Council, p. 365–374.

Egyptian Geological Survey and Mining Authority (EGSMA), 1981. Geologic map of Egypt 1:2000000. EGSMA, Cairo.

Egyptian Geological Survey and Mining Authority (EGSMA), 1992. Geological map of Sinai, A.R.E. Sheet No. 5, Scale 1:250,000.

Egyptian Geological Survey and Mining Authority (EGSMA), 1993. Geological map of Sinai, A.R.E. Sheet No. 4, Scale 1:250,000.

Egyptian Geological Survey and Mining Authority (EGSMA), 1994. Geological map of Sinai, A.R.E. Sheet No. 2 & 3, Scale 1:250,000.

El-Bohoty, M., Brimich, L., Saleh, A., Saleh, S., 2012. Comparative study between the structural and tectonic situation of southern Sinai, and red sea, Egypt, as deduced from magnetic, gravity, and seismic data. Nat. Res. Inst. Astron. Geophys., 357–388

Folkman, Y., Assael, R., 1980. Preparing of aeromagnetic map of Sinai, Egypt. The institute of petroleum research and geophysics, Israel.

Garcia, J.G., Ness, G.E., 1994. Inversion of the power spectrum from magnetic anomalies. Geophysics 59, 391–400.

Ghamry, E.M., 2002. Geophysical investigation of El-Hasana area North Sinai, Egypt. M.Sc Thesis, Al-Azhar University.

Hinze William, J., Von Frese, Ralph R.B., Saad, Afif H., 2013. Gravity and magnetic exploration Principles, Practices, and Applications. Cambridge university press. first published 2013.

Ismail, A.M., Sultan, S.A., Mohamady, M.M., 2001. Bouguer and Total Magnetic Intensity maps of Sinai Peninsula, Scale 1: 500,000. In: Proc. 2th International Symposium on Geophysics, Tanta, pp. 111–117.

Linsser, H., 1967. Investigation of tectonics by gravity detaling. Geophys. Prospecting. 15, 480–515.

Mekkawi, M., Elbohtoy, M., Aboud, E., 2007. Delineation of Subsurface Structures in the area of a Hot Spring, Central Sinai, Egypt based on Magnetotelluric and

Magnetic Data. In: Proceeding of the 8th Conf. Geology of Sinai for Development, Ismailia, 2007, pp.29–39.

Oasis Montaj Program v.8.4, 2015. Geosoft mapping and processing system, version 8.4, 2015.

Rabeh, T., 2011. Tectonic Model of the Sinai Peninsula Based on Geophysical Investigations. Tectonics. Fac. of Sci. Lisbon University, Portugal, pp. 93–100.

Reid, A.B., Allsop, J.M., Granser, H., Millett, A.J., Somerton, I.W., 1990. Magnetic interpretation in three dimensions using Euler Deconvolution. Geophysics 55, 80–90.

Said, R., 1962. The geology of Egypt. Elsevier Publishing Co., Amesterdam, New York, p. 377p.

Salem, A., Williams, S., Fairhead, D., Smith, R., Ravat, D., 2008. Interpretation of magnetic data using tilt angle derivatives. Geophysics 73, L1–L9.

Selim, E.I., Aboud, E., 2012. Determination of sedimentary cover and structural trends in the Central Sinai area using gravity and magnetic data analysis. J. Asian Earth Sci. 43 (2012), 193–206.

Spector, A., Grant, F.S., 1970. Statistical models for interpreting aeromagnetic data. Geophysics 35, 293–302.

Sultan, S.A., Mekhemer, Hatem M., Santos, F.A., Abd Alla, M., 2009. Geophysical Measurements for Subsurface Mapping and Groundwater Exploration at the Central Part of the Sinai Peninsula, Egypt., The Arabian Journal for Science and Engineering, vol. 34, Number 1A; 17P.

Tatiana, F.Q., Angelo, S., 1998. Exploration of a lignite bearing in Northern Ireland, using Maurizio ground magnetic. Geophysics 62 (4), 1143–1150.

Thompson, D.T., 1982. EULDPH- a new technique for making computer-assisted depth estimates from magnetic data. Geophysics 47, 31–37.